Journal of Applied Electrochemistry (2006)
DOI 10.1007/s10800-005-9110-y

Anodically grown films on copper and copper–nickel alloys in slightly alkaline solutions

F. BRIZUELA, R. PROCACCINI, S. CERÉ and M. VÁZQUEZ*
División Corrosión, INTEMA Facultad de Ingeniería, Universidad Nacional de Mar del Plata (UNMdP), Juan B. Justo 4302, B7608FDQ, Mar del Plata, Argentina
*(*author for correspondence, tel.: + 54-223-481-6600, fax: + 54-223-481-0046, e-mail: mvazquez@fi.mdp.edu.ar)*

Received 18 October 2005; accepted in revised form 14 December 2005

Key words: copper alloys, oxygen reduction, surface films

Abstract

Surface oxides grown on copper and copper–nickel alloys (UNS 72000 and UNS 70600) in aerated borax-borate buffer solution of pH 7.7 were characterized using various experimental techniques. Their influence on the mechanism of oxygen reduction was also investigated. The composition of the passive films formed *in situ* on the different materials was studied using differential reflectance spectroscopy. Electrochemical techniques such as voltammetry and potentiodynamic reductions, as well as hydrodynamic tools such as the rotating disk electrode were used to characterize the kinetic parameters of the oxygen reduction reaction. The results show that the addition of Ni to Cu to form copper–nickel alloys changes the composition of the surface film. As the amount of Ni in the alloy increases, the proportion of Cu(I) compounds decreases, and Ni(II) compounds are incorporated into the film structure. The films anodically grown at 0.5 V on Cu70Ni30 tend to be thinner but more resistive. This is supported by results from reflectance and impedance spectroscopy. The kinetics of oxygen reduction follows a four-electron path on surface-free films, independently of the Ni-content in the alloy.

1. Introduction

Copper, as well as many copper-based alloys are extensively used for constructing industrial equipment, particularly tubing systems and heat-exchangers [1–3]. The incorporation of nickel as an alloying element has proven to be beneficial, in terms of improving corrosion resistance to aggressive environments. The corrosion resistance of copper–nickel alloys is directly related to the performance of the passive film [4]. The film is mainly composed of Cu_2O but the incorporation of alloying elements can improve its properties.

The passive film also plays a key role in the mechanism of oxygen reduction, which constitutes the cathodic hemireaction of the corrosion process in aqueous aerated electrolytes [5, 6]. Different oxidation states of the same element or cations of diverse nature can enter into a catalytic cycle for the reduction of the important peroxide intermediate, as shown before. In the case of copper-based alloys, the presence of Cu(I) on the metallic surface appears to be essential in the reduction mechanism [7].

This study focuses on the influence of Ni as alloying element. Special attention was paid to the surface film formed and to the effect of varying amounts of the alloying element on the reaction kinetics. Boric-borate buffer (pH = 7.8) was chosen as electrolyte. The composition of the surface oxide layer on copper is well characterized in this electrolyte [8].

Other variables that also participate in the process, such as the presence of aggressive ions in solution, microorganisms and other contaminants in the water have been described elsewhere [9, 10].

2. Experimental setup

The electrodes were constructed from spectroscopic grade copper (99.99%) and from Cu90Ni10 (UNS 70600) and Cu70Ni30 (UNS 72000) provided by Metals Sample™, USA. For the stationary experiments, metal disks were embedded in epoxy resin and conveniently mounted on PVC holders. A cable for electrical contact was welded at the back side of the disk. To prepare rotating-disk electrodes, rods of Cu and Cu–Ni alloys were embedded in epoxy resin and mounted in Grilon™ cylindrical holders. Prior to the electrochemical analysis, the electrodes were abraded with a sequence of emery papers and finally mirror polished with 0.5 μm alumina powder.

The electrochemical measurements were conducted using a standard three-electrode cell. A Pt wire of large-enough area was used as auxiliary electrode. Two

different electrodes were used as reference: $Hg/Hg_2SO_4/K_2SO_4$ sat. (0.615 V vs NHE) for the electrochemical experiments and Ag/AgCl/NaCl 3 mol/l (0.281 V vs NHE) when recording reflectance spectra. However, to simplify comparisons, all the potential values will be indicated taking the saturated calomel electrode (SCE, $E = 0.242$ V vs NHE) as reference. The electrochemical instrumentation included a Voltalab PGP 201 potentiostat and a Solartron SI 1280B unit.

Boric-borate buffer (pH = 7.8) was used as electrolyte. All the experiments were carried out at room temperature (20 ± 2 °C). The oxygen content in air saturated solutions can be taken as 2.73×10^{-4} mol l^{-1} at 20 °C.

When cyclic voltammograms were recorded, the electrolyte was deaerated for 15 min with high-purity N_2 prior to each measurement. The electrodes were then pretreated by holding them at −1.0 V for 10 min to give a reproducible initial condition. Finally the scan was started at −0.8 V using a sweep rate of 0.01 V s^{-1} and reversed at 0.5 V.

Another group of experiments was performed after a surface film was anodically grown on the electrodes. The samples were prereduced at −0.8 V for 15 min and then the oxide grown holding them at 0.5 V for 30 min. To carry out the potentiodynamic reductions of the surface film the electrodes were immediately transferred to another cell where the oxides were reduced in deareated electrolyte applying a potentiodynamic scan from 0.5 to −1.0 V at a scan rate of 0.01 V s^{-1}. The starting point was the positive potential where the oxide had been grown, from where the potential was moved in the negative direction up to −1.1 V.

The oxygen reduction polarization curves were registered at 0.01 V s^{-1}, using five different rotation rates between 225 and 2025 rpm. The rotating disk experiments were carried out using a Radiometer™ controller (CTV101). The electrolyte was saturated with oxygen, bubbling the gas for at least 15 min prior to recording the polarization curves.

Electrochemical impedance spectroscopy (EIS) tests were performed at pre-reduced electrodes held a −1.0 V as well as at open circuit potential (OCP) on pre-oxidized electrodes. In this last case, the surface film was grown for 30 min at 0.5 V. The electrodes were then kept at OCP until the potential attained a stable value. Recording each spectrum took between 90 and 120 min. The solution was used without stirring or deareation. The AC voltage signal amplitude was ± 0.005 V_{rms} and the frequency was varied between 100 kHz and 1 mHz. The results were analyzed using equivalent circuits. The experimental data were fitted to each proposed equivalent circuit using ZView [11]. In the case of pre-reduced electrodes, the conventional Randles circuit gave satisfactory fittings.

The circuit chosen to fit the results on pre-oxidized electrodes is presented in Figure 1. This circuit is

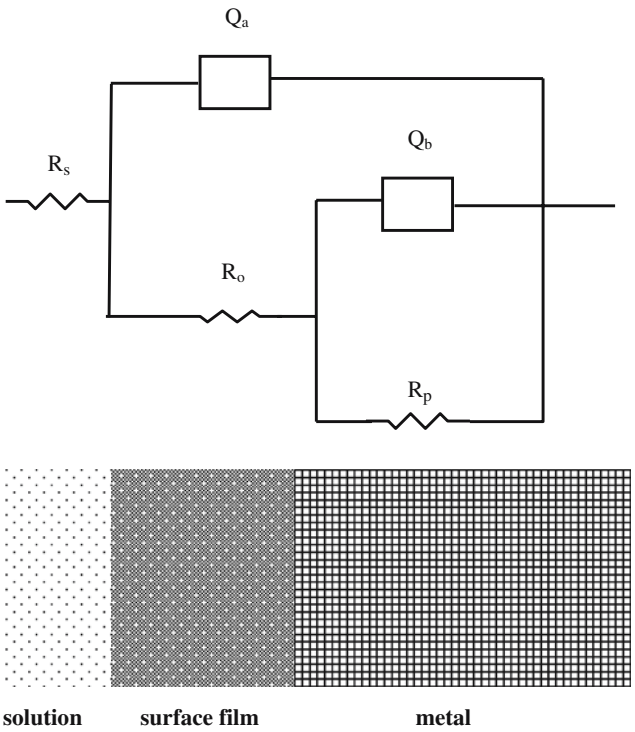

Fig. 1. Equivalent circuit proposed for interpreting the EIS response of pre-oxidized electrodes.

typical of oxide-coated metals and has been used before by other authors. Corroding electrodes can show various types of inhomogeneities, which can be represented by the inclusion of constant phase elements (CPE) in place of capacitors in the equivalent circuit. Surface roughness, insufficient polishing, grain boundaries and surface impurities have been mentioned among the main reasons allowing the use of CPEs in equivalent circuits of corroding electrodes [12]. The impedance of CPEs can be written as:

$$Z_{CPE} = [Q(j\omega)^n]^{-1} \quad (1)$$

where Q is the frequency-independent constant or pseudo-capacitance and n a constant power, with $-1 < n < 1$. A rough or porous surface can cause a double layer capacitance to appear as a constant phase element with n between 0.5 and 1.

The composition of the surface films was also evaluated using reflectance spectroscopy. The absorption spectra were recorded *in situ*. Baseline corrections were carried out by polarizing two identical polished surfaces at −1.0 V to prevent oxide growth. The spectrum of each surface was recorded after holding the electrodes at 0.5 V for 30 min in aerated electrolyte. The spectroelectrochemical measurements were carried out using a commercial double-beam spectrophotometer (Shimadzu UV 160A), appropriately modified as described elsewhere [13].

3. Results and discussion

3.1. *Characterization of the surfaces by cyclic voltammetry*

Figure 2 shows the cyclic voltammogram of copper and copper–nickel alloys in deaerated boric-borax buffer pH 7.8. Oxide growth starts at potentials positive to 0.1 V. A sharp anodic peak is clear, as well as two cathodic peaks which can be attributed to Cu(II) and Cu(I) reduction [4, 14]. At potentials positive to 0.5 V the electrodes tend to show localized corrosion. At potential values negative to −1.0 V the current increases due to water reduction. The three materials have similar voltammograms. No peak was observed which could be attributed to Ni species.

3.2. *Surface characterization by reflectance spectroscopy and potentiodynamic reduction*

Figure 3 presents the reflectance spectra typical of copper, Cu90Ni10 and Cu70Ni30 electrodes held at 0.5 V for 30 min. In the case of copper the absorbance peaks at 230 and 280 nm together with the shoulder at 560 nm are characteristic of Cu_2O [13, 15]. The main features of a differential reflectance spectrum of a Cu(I) oxide were first measured by Shanley et al. [15]. Cupric oxide, on the other hand, has a featureless absorption band, increasing in intensity as the wavelength approaches the UV-range [13, 15], which could also be detected in the copper electrodes. The spectra obtained for the two copper–nickel alloys are similar to those reported by other authors [13]. In the case of Cu90Ni10 the characteristic peaks of Cu_2O are, however, weaker. In the case of Cu70Ni30 the distinctive features of the Cu_2O spectrum are even weaker. The inclusion of Ni(II) oxide in the passive film could not be detected from the deconvolution of the spectra. CuO has a strong absorbance band very close to that of Ni(II) compounds. The incorporation of Ni(II) compounds into the surface film favours the formation of Cu(II) compounds. This can be observed in the Cu70Ni30 spectrum, comparing the relative intensities of the Cu(II)/Cu(I) peaks.

The difference in the transmittance values in the spectra in Figure 3 can be attributed to differences in the thickness of the surface films on each metal. The film on copper seems to be thicker. As the nickel content in the alloy increases, the thickness decreases because Cu(II) and Ni(II) oxides are more compact than Cu_2O. This overall change in the composition and thickness of the passive layer is related to the better corrosion resistance of Cu70Ni30.

The spectra in Figure 4 were obtained for surface films prepared as described for Figure 3, which were partially reduced for 15 min at −0.3 V. As suggested by the results in Figure 2, Cu(II) species should be reduced at this potential while the resulting Cu(I) species are incorporated to the film. As the Ni content in the metal base increases the characteristic features of the Cu_2O spectrum are lost. This fact may be interpreted as the stabilization of Cu(II) species in the film promoted by the incorporation of Ni(II) compounds into the passive layer.

When the films that grow on Cu and Cu90Ni10 after 30 min at 0.5 V are potentiodynamically reduced, two cathodic peaks appear in each case, in good agreement

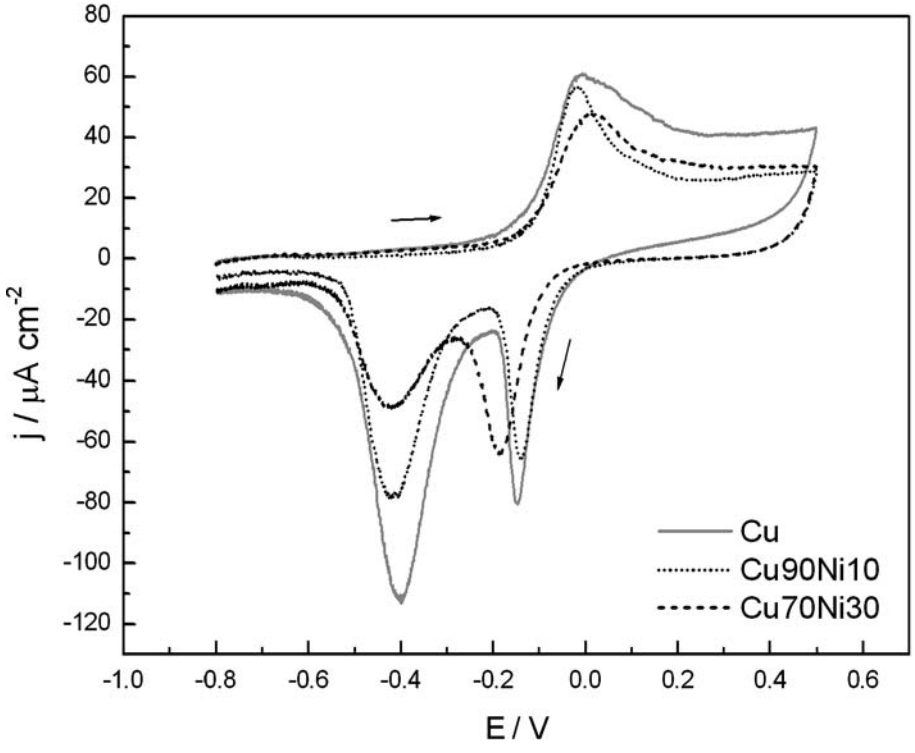

Fig. 2. Voltammetry of Cu, Cu90Ni10 and Cu70Ni30 electrodes in contact with deaerated boric-borate buffer pH 7.8 ($v = 0.01$ V s^{-1}).

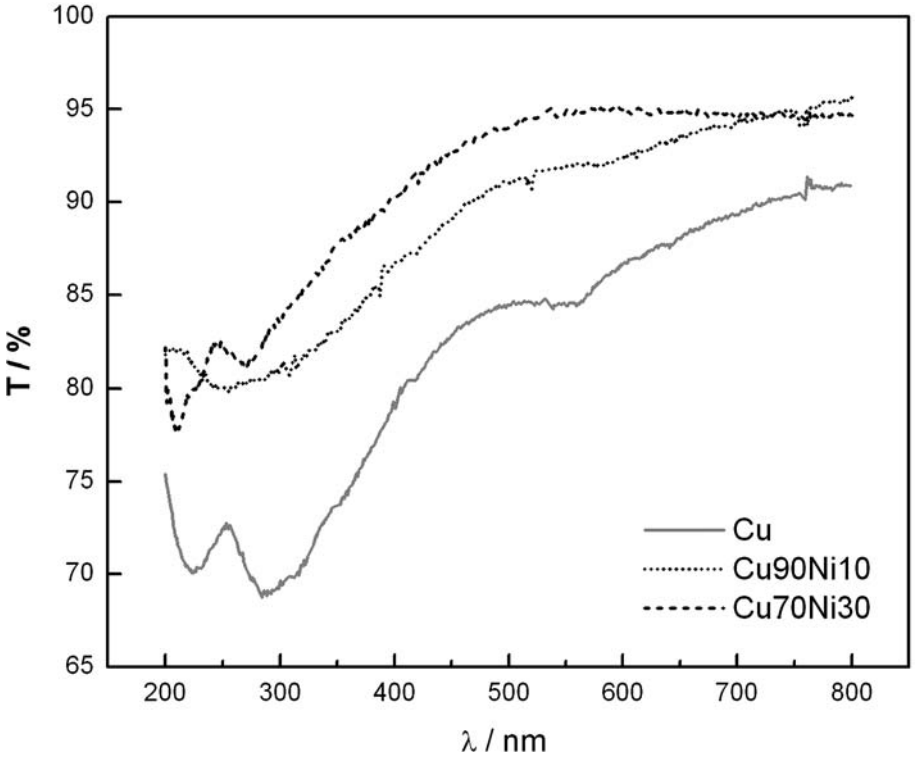

Fig. 3. Differential reflectance spectra for Cu, Cu90Ni10 and Cu70Ni30 in aerated boric-borate buffer solution pH 7.8 after holding them at 0.5 V for 30 min.

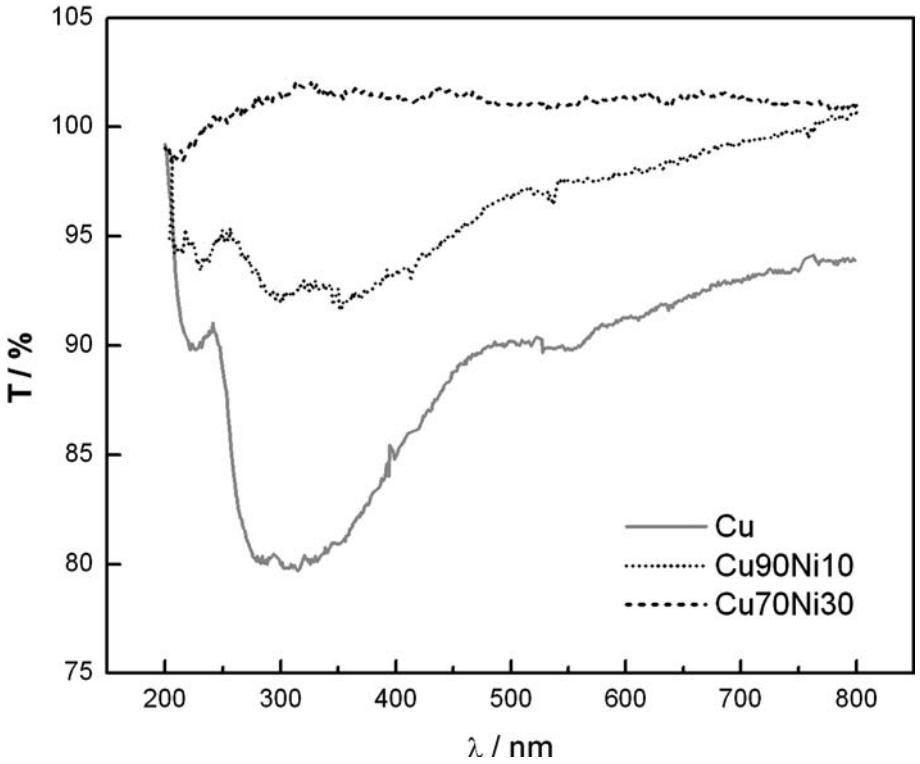

Fig. 4. Differential reflectance spectra for Cu, Cu90Ni10 and Cu70Ni30 in aerated boric-borate buffer solution pH 7.8. After recording the spectra in Figure 3, the electrodes were held at −0.3 V for 30 min.

with those found in the voltammograms shown in Figure 2. When the areas of the two peaks are compared it can be seen that the proportion of Cu(I)/Cu(II) compounds is lower in the case of the alloy. In the case of Cu70Ni30, three cathodic peaks appear when the surface film is reduced (see Figure 5). The new peak

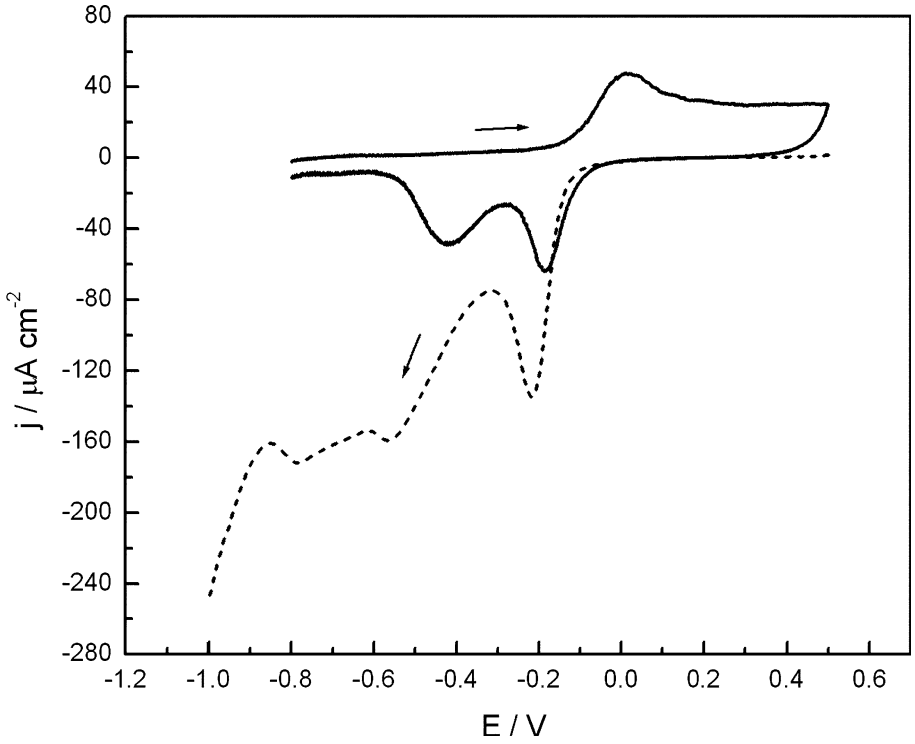

Fig. 5. Cu70Ni30 voltammetry (same as Figure 2), dot line. Potentiodynamic reduction curve of the oxides formed during 30 min. at 0.5 V, full line. The curves are registered in deaerated boric-borate buffer pH 7.8 at 0.01 V s^{-1}.

at −0.8 V could be attributed to NiO reduction, in agreement with the results from independent experiments, presented above.

3.3. *Surface films characterization by electrochemical impedance spectroscopy*

Impedance spectra were recorded on copper and copper–nickel electrodes held at −1.0 V (clean surface) and 0.5 V (passive surface). The results, in the form of Bode plots, are shown in Figures 6 and 7 for clean and oxidized surfaces, respectively.

The spectra obtained for clean, reduced surfaces can be fitted using a simple Randles equivalent circuit. The fitting parameters are presented in Table 1.

When the surface film grown at 0.5 V is present on the metallic surface the impedance spectra present two time constants. A schematic representation of the structure of the surface film present on the metallic surfaces after passivation, as well as the corresponding equivalent circuits is shown in Figure 1. EIS data fit results are shown in Figure 6 and 7, together with the recorded data. R_s represents the solution resistance, Q_a the pseudo-capacitance of the surface oxide, R_o the resistance to current flow through defects in the surface oxide, Q_b the metal pseudo-capacitance and R_p the polarization resistance. The experimental data were found to be sufficiently well fitted by the proposed equivalent circuit. The fitting parameters are presented in Table 1 which suggest that the increase in the oxide pseudo-capacitance (Q_a) of the film with the increase in the Ni content in the alloy may be attributed to a thinner

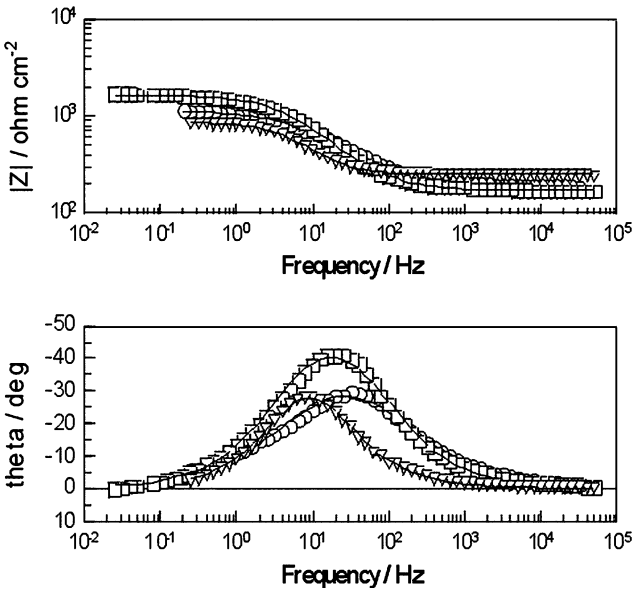

Fig. 6. Impedance spectra using the Bode representation recorded on Cu (O), Cu90Ni10 (□) and Cu70Ni30 (▽) electrodes held at −1.0 V. The symbols represent the data and the lines the fitting results. During the fitting procedure, the Randles equivalent circuit has been employed.

superficial film, in good agreement with the results obtained by reflectance.

3.4. *Cathodic polarization curves under hydrodynamic control*

Cathodic polarization curves were registered on clean surfaces using rotating disk electrodes, as described in

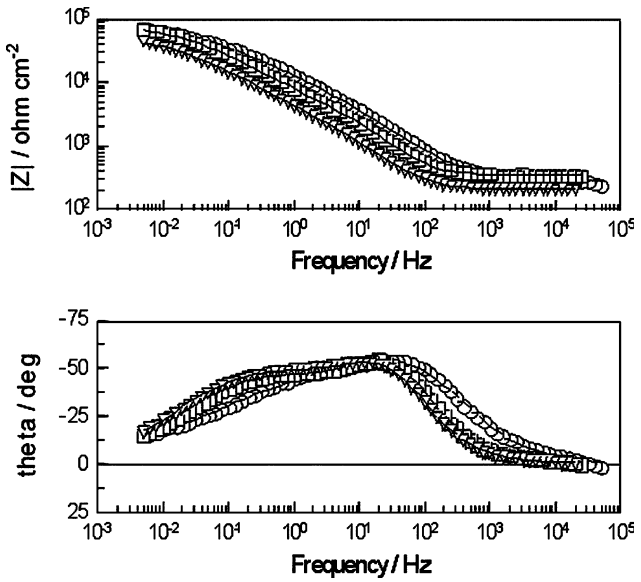

Fig. 7. Impedance spectra using the Bode representation recorded at OCP on Cu (O), Cu90Ni10 (□) and Cu70Ni30 (▽) electrodes held at 0.5 V for 30 min. The symbols represent the data and the lines the fitting results. During the fitting procedure, the equivalent circuit presented in Figure 1 has been employed.

Section 2. A typical result for Cu is presented in Figure 8. Two distinctive regions can be defined: a potential range of mixed control (activated and diffusional), where current and potential are interdependent and a diffusional range at more negative potentials, where the current is no longer dependent on the potential values. The final current increase in the negative end of the potential interval is due to water decomposition. The curves registered for the other materials present similar characteristics. The number of electrons exchanged in the cathodic hemireaction can be calculated from the slope of the appropriate representation of the Levich equation [16]

$$j_L = 0.20nFD^{2/3}\nu^{-1/6}C_B\omega^{1/2} \quad (2)$$

where j_L is the limiting current density, D the diffusion coefficient of the electroactive species in $cm^2\ s^{-1}$, ν is the kinematic viscosity in $cm^2\ s^{-1}$, C_B represents the oxygen concentration in the bulk solution in mol dm^{-3}, and ω is the rotation rate in rpm.

For all three of the materials under investigation, in the pre-reduced condition, the slope of the j_L vs $\omega^{1/2}$ plot is approximately 30 $\mu A\ cm^{-2}\ rpm^{-1}$. This slope value was calculated taking the concentration of oxygen in the air saturated solution as $2.73\times\ 10^{-4}$ mol l^{-1}, the kinematic viscosity as 0.01 $cm^2\ s^{-1}$ and the diffusion coefficient as $1.9 \times 10^{-5}\ cm^2\ s^{-1}$. The number of electrons calculated for each material is shown in Table 2. An exchange of four electrons can be explained if the oxygen reduction follows a direct path, with no hydrogen peroxide formation as reaction intermediate.

In the mixed controlled range of the polarization curves, the Koutecky–Levich equation (Eq. 3) can be used [16]

$$\frac{1}{j} = \frac{1}{j_A} + \frac{1}{0.20nFD_R^{2/3}\nu^{-1/6}C_R^*\omega^{1/2}} \quad (3)$$

where the symbols have the same meaning as those used in Eq. (2).

The number of electrons exchanged as a function of the applied potential, can be calculated from the slope of the j^{-1} vs $\omega^{-1/2}$ representation. The results for the pre-reduced electrodes can be seen in Figure 9. The difference in the values of n may be attributed to the presence of residual oxides, which form naturally on corrodible metals and cannot be reduced during the preconditioning treatment.

Polarization curves were also registered on electrodes where a surface film had been anodically grown by polarizing it at 0.5 V for 30 min. The curves started at 0.5 V and the potential was swept in the negative direction. A set of typical curves is presented in Figure 8, superimposed to those for clean, reduced electrodes. A much narrower diffusional interval is now evident. The diffusional current density in the cathodic current is slightly higher for the oxidized electrodes. This is not surprising, as it represents the simultaneous reduction of oxygen and surface oxides. However, in the mixed control range the current density registered for those electrodes where a surface film has been grown is always lower when compared to clean electrodes. When the amount of nickel in the alloy increases, the difference in the currents also increases. This has been represented in Figure 10 by plotting the quotients $j_{L\ ox}/j_{L\ clean}$ at −0.3 V and for various rotation rates. This supports the idea of a more compact and resistive film as the amount of Ni increases. An increase in resistance following the increase in Ni content has been found by other authors [17]. They

Table 1. Optimized values for the parameters employed in fitting the data in Figures 6 and 7 to the equivalent circuit proposed in Figure 1

Element	Cu −1.0 V	Cu90Ni10 −1.0 V	Cu70Ni30 −1.0 V	Cu 0.5 V	Cu90Ni10 0.5 V	Cu70Ni30 0.5 V
$R_s/\Omega\ cm^2$	259.5	166.3	253.9	268.2	251.8	224.5
$Q_a/\Omega^{-1}\ cm^{-2}\ s^n$	–	–	–	7.63	15.8	25
n_a	–	–	–	0.79	0.88	0.85
$R_o/\Omega\ cm^2$	–	–	–	1777	3825.5	2504.4
$Q_b/\Omega^{-1}\ cm^{-2}\ s^n$	74.7	74.8	93.0	42.4	65.8	70.4
n_b	0.67	0.82	0.84	0.39	0.63	0.71
$R_p/\Omega\ cm^2$	1007	1454.5	661.9	122321	38326	47694

Each value corresponds to, at least, an average of three independent measurements.

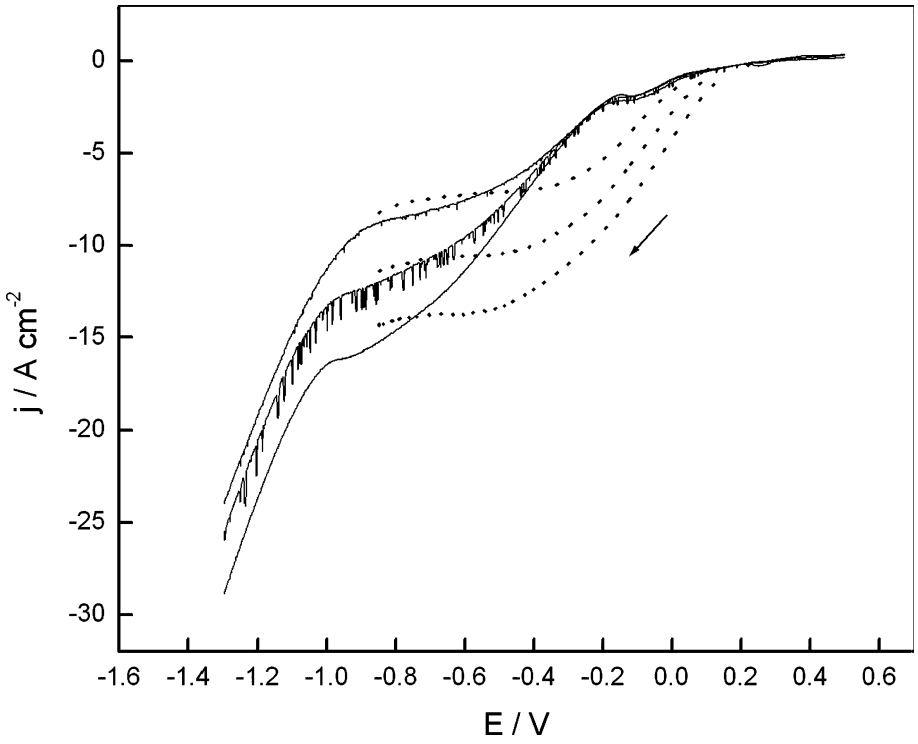

Fig. 8. RDE polarization curves for Cu electrodes pre-reduced at −0.8 V during 15 min (dots line) and Cu70Ni30 electrodes pre-oxidized at 0.5 V for 30 min (full line). Curves started at −1.3 V. Rotation rates are 400, 900 and 1600 rpm. Scan rate: 0.01 mV s^{-1}.

propose that the extensive incorporation of Ni(II) to the surface film would lead to a higher ionic and electronic resistance, leading to a structure containing less defects. This interpretation is also supported by field experience, where a better performance of Cu70Ni30 against corrosion has been found for slightly alkaline environments [1].

4. Conclusions

The addition of Ni to Cu, to form copper–nickel alloys, changes the composition of the film anodically grown at 0.5 V in borax buffer pH 7.8. As the amount of Ni in the alloy increases, the proportion of Cu(I) compounds in relation to Cu(II) ones decreases, together with the incorporation of Ni(II) compound into the film structure. When more nickel is incorporated into the alloy composition, anodically grown films at 0.5 V tend to be thinner. This is supported by results from reflectance and impedance spectroscopy.

Table 2. Number of electrons exchanged in the oxygen reduction reaction evaluated from the limiting current density and the Levich equation (average of three independent measurements)

Material	n (electrons)
Cu	4.05 ± 0.28
Cu90Ni10	3.74 ± 0.36
Cu70Ni30	4.01 ± 0.03

The electrodes were pre-reduced at −0.8 V.

The kinetics of oxygen reduction follows a four-electron path on surface-free films, independently of the Ni-content in the alloy. In the presence of a surface film, the limiting current for oxygen reduction is poorly defined, because of the current due to oxide reduction, which is superimposed in the same potential range. If oxygen reduction is under mixed control (activation and diffusional) the current is always lower as the Ni content increases, in good agreement with the presence of a more resistive surface.

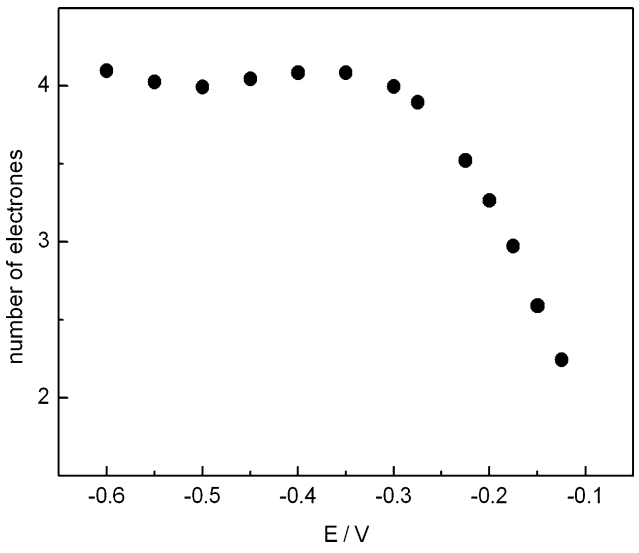

Fig. 9. Electrons (n) exchanged in the oxygen reduction reaction on pre-reduced Cu70Ni30, calculated from the Koutecky–Levich equation as a function of the applied potential.

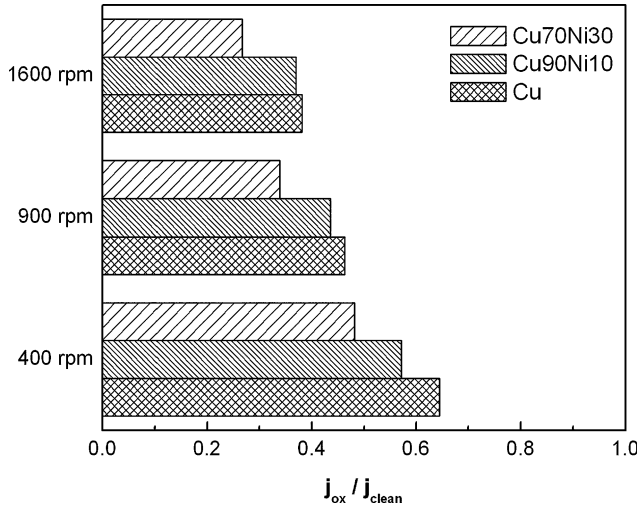

Fig. 10. Quotient between the limiting current for oxidized and pre-reduced electrodes, evaluated at −0.3 V for Cu, Cu90Ni10 and Cu70Ni30.

Acknowledgements

The authors acknowledge the financial support received from the National Research Council of Argentina, CONICET, (Project PIP 02570) and from the Universidad Nacional de Mar del Plata (Project 15/G115).

References

1. S.R. de Sanchez, *Corros. Rev*. **VIII** (1989) 283.
2. C. Manfredi, S. Simison and S.R. de Sánchez, *Corrosion* **43** (1987) 458.
3. S.R. de Sánchez and D.J. Schiffrin, *Corros. Sci.* **22** (1982) 585.
4. S. Ceré and M. Vázquez, *J. Mater. Sci. Lett*. **21** (2002) 493.
5. M.V. Vazquez, S.R. de Sánchez, E.J. Calvo and D.J. Schiffrin, *J. Electroanal. Chem*. **374** (1994) 179.
6. M.V. Vazquez, S.R. de Sánchez, E.J. Calvo and D.J. Schiffrin, *J. Electroanal. Chem*. **374** (1994) 189.
7. S. Ceré, M. Vazquez, S.R. de Sánchez and D.J. Schiffrin, *J. Electroanal. Chem*. **505** (2001) 118.
8. H.D. Speckmann, M.M. Lorenghel, J.W. Schultze and H.H. Strehblow, *Ber. Bunsenges, Phys. Chem*. **889** (1985) 392.
9. M. Vazquez and S.R. de Sanchez, *J. Appl. Electrochem*. **28** (1998) 1383.
10. J.P. Busalmen, M. Vazquez and S.R. de Sánchez, *Electrochim. Acta* **47** (2002) 1857.
11. I. Scribner Associates, *ZPlot for Windows* (1998).
12. L.J. Aljinovic, S. Gudic and M. Smith, *J. Appl. Electrochem*. **30** (2000) 973.
13. S.R. de Sánchez, L.E.A. Berlouis and D.J. Schiffrin, *J. Electroanal. Chem*. **307** (1991) 73.
14. H.H. Strehblow and H.D. Speckmann, *Werks und Korros* **35** (1984) 512.
15. C.W. Shanley, R.E. Hummel and E.D.V. Verink Jr., *Corros. Sci.* **20** (1980) 481.
16. A.J. Bard and L.R. Faulkner, *Electrochemical Methods, Fundamentals and Applications* (Wiley, New York, 1980).
17. R.F. North and M.J. Pryor, *Corros. Sci.* **9** (1969) 509.